First published in:
Annals of Biomedical Engineering, Vol. 29, pp. 483–492, 2001
Printed in the USA. All rights reserved.
0090-6964/2001/29(6)/483/10/$15.00

Classification of Endocardial Electrograms Using Adapted Wavelet Packets and Neural Networks

DANIEL STRAUSS,[1] JENS JUNG,[2] ANDREAS RIEDER,[3] and YIANNOS MANOLI[4]

[1]Applied Mathematics and Computer Science, University of Mannheim, D-68131 Mannheim, Germany, [2]Internal Medicine III, University Hospital, D-66421 Homburg/Saar, Germany, [3]Institute for Scientific Computing and Mathematical Modeling, University of Karlsruhe, D-76128 Karlsruhe, Germany, and [4]Institute of Microelectronics, University of Saarland, D-66041 Saarbrücken, Germany

(Received 9 May 2000; accepted 26 February 2001)

Abstract—The discrimination of ventricular tachycardias with 1:1 retrograde conduction from sinus tachycardia still remains a challenge for rate based algorithms commonly used in dual-chamber implantable cardioverter defibrillators. Morphology based analysis techniques for a classification of antegrade and retrograde atrial activation patterns can be used to cope with this problem. Here time-domain template matching techniques are known approaches. However, a time-domain representation of endocardial electrograms is not optimal for classification tasks as the dimensionality of the underlying signal space is high and features being irrelevant for a signal characterization are involved in the analysis. Therefore, the aim of this study is to develop an enhanced morphological analysis tool for a classification of antegrade and retrograde atrial activation by using a transform domain representation of endocardial electrograms. For this, we applied an adapted wavelet-packet decomposition to extract discriminating features in endocardial electrograms representing antegrade and retrograde activation patterns. Further, a feed-forward neural network was utilized to produce a classification based on the extracted information. In using our hybrid method, no false classification of the physiological and pathological cardiac state was made. It is concluded that the proposed classification scheme represents a highly efficient approach for a classification of antegrade and retrograde atrial activation. © *2001 Biomedical Engineering Society.*
[DOI: 10.1114/1.1376409]

Keywords—Endocardial electrograms, Dual-chamber ICDs, Adapted wavelet packets, Filter banks, Neural networks.

INTRODUCTION

The implantable cardioverter-defibrillator (ICD) is accepted to be the most effective therapy for preventing sudden cardiac death due to ventricular tachycardias (VT).[19] Such a device is continually monitoring the electrical activity of the heart, represented by an endocardial electrogram, and delivers defibrillation and/or pacing therapy if a life-threatening arrhythmia is detected. Conventionally, an endocardial electrogram is obtained from a single ventricular lead and analyzed in view of the ventricular rate by the ICD. Although detection enhancements like *rate stability* or *sudden onset* are used in third generation ICD systems, inappropriate ICD therapy occurs in up to 13% of the patients who received such a device.[17,28] Whether the use of the recently introduced dual-chamber ICDs[14] will lead to a reduction of inadequate therapies is currently under investigation. Such a dual-chamber system also analyzes an atrial endocardial electrogram (AEE) obtained from an additional atrial lead.

A major challenge for rate based algorithms commonly used in dual-chamber ICD-systems is the discrimination of VT with 1:1 retrograde conduction from sinus tachycardia due to a correspondence of the atrial and the ventricular rate. It is known, that the morphology of antegrade and retrograde atrial activation patterns can be used when a rate independent discrimination of the physiological from the pathological cardiac state is needed.[22,23] Here time-domain template matching methods such as the correlation waveform analysis,[22] the area of difference,[21] or the bin area method[20] are possible approaches.

In Leong and Jabri[12] a classification scheme called morphology and timing intracardiac classifier (MATIC) is proposed which analyzes the morphology of endocardial electrograms additionally to rate criteria for patients having VT with 1:1 retrograde conduction. MATIC uses a neural network to perform the template matching task.

All methods mentioned so far are based on the time-domain representation of endocardial electrograms, that is, the classification is directly applied to the original—and often high dimensional—signal space. Therefore, we aimed at the construction of a feature extractor which performs a mapping from the original signal space onto a lower dimensional feature space where the discriminating information of patterns belonging to distinct classes appear clearly. Appropriate feature extractors can significantly reduce the dimensionality of the problem and en-

Address correspondence to Daniel Strauss, University of Mannheim, Building D7, 27, Room 401, D-68131 Mannheim, Germany. Electronic mail: strauss@keynumerics.com

hance the performance of the classifier. Recently, the superiority of feature extraction based on orthonormal wavelet-type (wavelet/wavelet packet) decompositions before the classification over the direct application of the classifier on the original signal was shown.[6,16] With such a decomposition technique, the signal is decomposed into a set of orthonormal basis functions (also called atoms) which are localized in the time-frequency plane. The application of such basis functions for feature extraction stems from the fact, that most of the signal features, e.g., the dominant morphologies in electrocardiograms (P, QRS, and T wave) are simultaneously localized in time and frequency. Therefore, wavelet-type decompositions are suitable for a variety of applications dealing with nonstationary signals as electrograms.[7–9] Recently, we have applied orthonormal wavelet-type decompositions of endocardial electrograms for the automatic discrimination of atrial tachyarrhythmias[12] and the detection of ventricular tachycardias.[8]

This paper presents an automatic neural network based classification scheme using adapted wavelet-packet decompositions for the extraction of discriminating scale features in AEEs representing antegrade and retrograde activation patterns.

METHODS

Data Acquisition

The signals used in our study were recorded during a clinically indicated electrophysiological examination in the laboratory of electrophysiology at the University Hospital in Homburg/Saar, Germany. The patient population studied here can be separated into two groups:

The first group with typical atrioventricular (AV) nodal tachycardia, studied as a model for patients having a spontaneous retrograde activation, was referred to the institution for radiofrequency ablation.

The second group with clinical monomorphic VT was referred to the institution for either electrophysiological study or radiofrequency ablation. In these patients, the evidence of an accessory pathway or dual AV nodal physiology was ruled out during the electrophysiological examination.

A written consent was obtained from all patients prior to the study. In both groups, bipolar endocardial signals were obtained from the high right atrium using the distal pair of a 6-French quadripolar electrode catheter with an interelectrode spacing of 0.5 cm (USCI, Bard, Billerica, MA). These AEEs were recorded during sinus rhythm and induced or spontaneously occurring AV nodal tachycardia or during induced monomorphic VT with 1:1 retrograde conduction. The endocardial recordings were amplified (HBV 20, Biotronik, Berlin, Germany), bandpass filtered (40–500 Hz) and digitized at 2 kHz with a 12 bit resolution (DT 2824-PGH, Data Translation, Marlboro, MA). Data segments of 10 s duration were stored for subsequent analysis.

Feature Extraction Using Adapted Wavelet-Packet Decompositions

The feature extraction scheme proposed in this paper is based on adapted wavelet-packet decompositions. Here the term *adapted* means that the wavelet-packet basis is chosen with respect to the AEE morphology of the individual patient.

Beat Selection. Consecutive beats within each recorded AEE were selected by threshold application in the time domain. A reliable detection threshold α was defined by 27% of largest sample amplitude of each data segment. After detection, i.e., the value α was crossed, each beat was fixed within a selection window of 128 ms which ranged from 40 ms before to 88 ms behind the crossing point of α. Due to our sampling frequency of $f_s = 2000\,\mathrm{Hz}$, a selected beat is therefore represented by $K = 256$ samples. To obtain a representative atrial activation pattern, we averaged five beats. Let us consider this pattern as a sequence belonging to the original signal space $\mathcal{S} \subset \mathbb{R}^K$. We used the wrap-around technique[18] for applying filter banks on such signal spaces of a finite dimension.

The Wavelet-Packet Basis. It is well known, that wavelet-type orthonormal decompositions can be realized by using finite impulse response (FIR) normalized paraunitary (NP) two-channel filter banks[24,26]—a class of perfect reconstruction filter banks—as building blocks in a tree-structured filter bank (as usual, we assume here the very same two-channel filter bank with a zero mean highpass filter on each decomposition level in tree). Note that the FIR property of the filters is equivalent to the use of basis functions with a compact support (that is, a finite duration), a necessary condition for capturing features being compact in time. Let P and Q be decomposition operators which are associated with the decimators of a two-channel NP analysis bank, P: lowpass (channel 0), Q: highpass (channel 1). Their adjoint operators, which are associated with the interpolators of the synthesis bank, are denoted by P^* and Q^*, respectively. Please see Fig. 1 for an illustration and the nomenclature for the mathematical definitions of decimators and interpolators. Due to the use of NP filter banks we have that

$$PQ^* = QP^* = 0 \quad \text{and} \quad P^*P + Q^*Q = I,$$

where I is the identity operator on $\mathbb{R}^K$. Now let $\Omega_{0,0}$ denote our signal space $\mathcal{S}$. Suppose further, that two-channel NP filter banks are arranged in a binary tree.

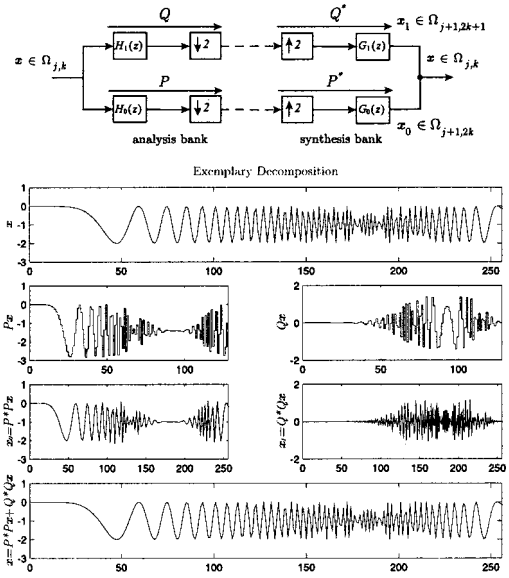

FIGURE 1. A two-channel NP building block and a decomposition example of a signal which contains different frequency components over time. $H_0(z)$ represents the analysis lowpass filter associated with the decomposition operator P and $H_1(z)$ the analysis highpass filter associated with the decomposition operator Q.

Then, the space $\Omega_{0,0}$ is successively decomposed into mutually orthogonal subspaces by P and Q such that

$$\Omega_{j,k}=\Omega_{j+1,2k}\oplus\Omega_{j+1,2k+1}$$

$$\text{for } j=0,1\ldots,J,\quad k=0,\ldots,2^j-1.$$

Schematically, this splitting is shown in Fig. 1 for a two-channel NP building block. In other words, let $\mathbf{x}=\{x[n]\}_{n=0}^{N-1}$ be the input sequence of a two-channel building block, then $P\mathbf{x}$ and $Q\mathbf{x}$ are two sequences with a lower resolution as $\mathbf{x}$ of the lengths $N/2$. In general, the sequence $P\mathbf{x}$ represents coarse morphological features of $\mathbf{x}$ whereas $Q\mathbf{x}$ represents fine or detail ones. The reconstructed versions of these sequences which have the same length as the input sequence are obtained by applying P^* and Q^*, respectively.

When using a frequency-domain consideration, a two-channel building block decomposes the bandwidth of the input signal into two subbands with uniform frequency bands. We can roughly say, that the input frequency band is halved.

The filter bank tree which makes up the backbone of our feature extraction scheme is shown in Fig. 2. In view of the preprocessing of the given data segments and features, especially the dimension of the feature space that we aimed at, this tree turned out to be well suited for our task. The tree with the output sequences $\mathbf{y}_m$, $m=1,2\ldots,8$ gives the following decomposition:

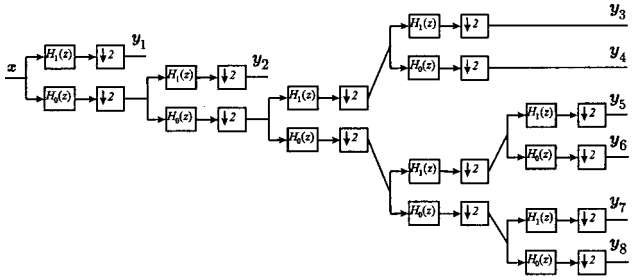

FIGURE 2. The filter bank implementation of our wavelet-packet decomposition.

$$(\mathbf{y}_1,\ldots,\mathbf{y}_8)=(Q\mathbf{x},QP\mathbf{x},Q^2P^2\mathbf{x},PQP^2\mathbf{x},Q^2P^3\mathbf{x},PQP^3\mathbf{x},QP^4\mathbf{x},P^5\mathbf{x}). \quad (1)$$

Features. Let $\mathcal{F}$ be our low dimensional feature space. For a characterization of atrial activation patterns we extracted a feature vector $\boldsymbol{\xi}\in\mathcal{F}$ by

$$\boldsymbol{\xi}=(\xi_1,\ldots,\xi_6):=(\|\mathbf{y}_3\|_{\ell^1},\ldots,\|\mathbf{y}_8\|_{\ell^1}), \quad (2)$$

so we have $\dim\mathcal{F}=6$. The vector $\boldsymbol{\xi}$ carries the concentration of $\mathbf{x}$ in ℓ^1 on level $m=3,\ldots,8$, i.e., the considered decomposition stages. Please note that we have discarded the sequences $\mathbf{y}_1$ and $\mathbf{y}_2$. They represent noise and/or very detailed morphological features of $\mathbf{x}$ and do not carry substantial discriminating features of the recorded AEEs representing the distinct activation patterns, please see Fig. 5 in the results for a graphic example. Therefore, these levels were considered to be irrelevant for our task. We normalized $\boldsymbol{\xi}$ such that $\|\boldsymbol{\xi}\|_{\ell^1}=1$ since we are only interested in the distribution of features in $\mathcal{F}$, i.e., the specific concentration on particular levels, and not in their overall energy content.

The whole process described so far is simply a map

$$f:\mathcal{S}\to\mathcal{F}.$$

The map f is called a feature extractor. In the following we will introduce our adaptation concept. For this, it is necessary to distinguish between feature vectors representing antegrade and retrograde activation patterns. Therefore, we will use notation $\boldsymbol{\xi}^{\text{ant}}$ and $\boldsymbol{\xi}^{\text{ret}}$ if the underlying pattern $\mathbf{x}$ originates from an antegrade activation and a retrograde one, respectively.

Adaptation of the Decomposition. So far, we are able to characterize antegrade and retrograde atrial activation patterns by relatively small feature vectors. However, there is no guarantee that $\boldsymbol{\xi}$ represents discriminating signal features in the distinct activation patterns when using arbitrary two-channel NP building blocks in the tree. Therefore, an adaptation of these building blocks

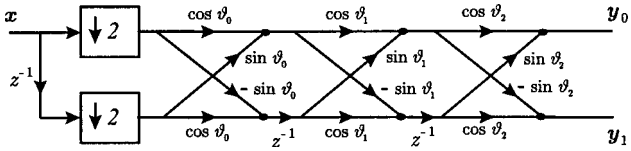

FIGURE 3. The parameterized lattice structure implementation of the NP analysis bank; *x*: input sequence; y_0: lowpass output; y_1: highpass output.

was realized such that $\boldsymbol{\xi}$ captures the morphological dissimilarities. For this, we used the lattice structure[24,25] which provides an efficient implementation and complete parameterization of all two-channel FIR NP filter banks with real filter coefficients. We parameterized filters of order $N=5$ which proved to be suitable for AEE decompositions.[7,8] To obtain the corresponding structure, the polyphase matrix of the analysis bank was decomposed in the following manner:

$$\mathbf{H}_{\mathrm{pol}}(z)=\mathbf{R}_2\mathbf{D}(z)\mathbf{R}_1\mathbf{D}(z)\mathbf{R}_0, \tag{3}$$

where

$$\mathbf{D}(z)=\mathrm{diag}[1,z^{-1}]$$

and

$$\mathbf{R}_i=\begin{pmatrix}\cos\vartheta_i & \sin\vartheta_i\\ -\sin\vartheta_i & \cos\vartheta_i\end{pmatrix},\quad i=0,1,2.$$

It can be verified that the polyphase matrix $\mathbf{H}_{\mathrm{pol}}(z)$ in Eq. (3) is in fact NP since we have a product of a rotation matrix $\mathbf{R}_i$ which is orthogonal and a delay matrix $\mathbf{D}(z)$ which is NP, i.e., $\mathbf{D}(z)\tilde{\mathbf{D}}(z)=\mathbf{I}$, where $\mathbf{I}$ is a 2×2 identity matrix and $\tilde{\mathbf{D}}(z)$ denotes the paraconjugate of $\mathbf{D}(z)$. The parameterized lattice structure is shown in Fig. 3.

Note, if $\cos\vartheta_i\neq 0$ for all i then $\cos\vartheta_i$ can be factored out and summarized to a common factor of the lattice structure. In this way we obtain the *two multiplier QMF lattice*[24] which is more efficient as the number of multiplications is reduced.

It is known, that the angles in Eq. (3) must add to $\pi/4$ to guarantee a highpass filter with a zero mean,[4,18] a necessary constraint for NP filter banks used for wavelet-type expansions. Thus, with the representation

$$\vartheta_2=\frac{\pi}{4}-\vartheta_0-\vartheta_1, \tag{4}$$

the angles $\boldsymbol{\vartheta}=(\vartheta_0,\vartheta_1)$ are the design parameters for the filter bank and, hence, for our complete wavelet-packet basis. For a numerical optimization, we considered the corresponding parameter space on a discrete grid. Let the set $\mathcal{P}$ be a sampling in $[0,\pi[$, that is,

$$\mathcal{P}=\left\{\frac{\pi\sigma}{T}\,\middle|\,\sigma=0,\ldots,T-1\right\},\quad T\in\mathbb{N}.$$

Our parameter space on a discrete grid is simply the two-fold Cartesian product of $\mathcal{P}$:

$$\mathcal{P}^2=\{\boldsymbol{\vartheta}=(\vartheta_0,\vartheta_1)\mid\vartheta_0,\vartheta_1\in\mathcal{P}\}. \tag{5}$$

We worked with $T=30$ for constructing $\mathcal{P}$. In this way, we achieved the discrete parameterization of our decomposition scheme. The extracted feature vector depends now on the angles $\boldsymbol{\vartheta}$.

Optimization Criterion. To determine the optimal wavelet-packet basis, we need a discriminant information functional which measures the dissimilarity among $\boldsymbol{\xi}^{\mathrm{ant}}(\boldsymbol{\vartheta})$ and $\boldsymbol{\xi}^{\mathrm{ret}}(\boldsymbol{\vartheta})$. For this, we applied the *J divergence*[16] (that is a symmetric version of the well known *Kullback–Leibler divergence*),[15] which is defined as

$$J[(\boldsymbol{\xi}^{\mathrm{ant}}(\boldsymbol{\vartheta}),\boldsymbol{\xi}^{\mathrm{ret}}(\boldsymbol{\vartheta}))]:=\sum_{n=1}^{\dim\mathcal{F}}\xi_n^{\mathrm{ant}}(\boldsymbol{\vartheta})\log\frac{\xi_n^{\mathrm{ant}}(\boldsymbol{\vartheta})}{\xi_n^{\mathrm{ret}}(\boldsymbol{\vartheta})}+\sum_{n=1}^{\dim\mathcal{F}}\xi_n^{\mathrm{ret}}(\boldsymbol{\vartheta})\log\frac{\xi_n^{\mathrm{ret}}(\boldsymbol{\vartheta})}{\xi_n^{\mathrm{ant}}(\boldsymbol{\vartheta})}, \tag{6}$$

with the convention $\log 0=-\infty$, $\log(\gamma/0)=\infty$ for $\gamma>0$, $0(\pm\infty)=0$. To optimize the decomposition for the individual patient, specific angles $\hat{\boldsymbol{\vartheta}}\in\mathcal{P}^2$ were chosen by

$$\hat{\boldsymbol{\vartheta}}=\mathrm{argmax}\{J[\boldsymbol{\xi}^{\mathrm{ant}}(\boldsymbol{\vartheta}),\boldsymbol{\xi}^{\mathrm{ret}}(\boldsymbol{\vartheta})]\,|\,\boldsymbol{\vartheta}\in\mathcal{P}^2\}. \tag{7}$$

Using $\hat{\boldsymbol{\vartheta}}$ in a future monitoring of the individual patient, our decomposition scheme will produce a different distribution of the features in $\mathcal{F}$ for the distinct activations. The described feature extraction algorithm can be summarized as follows.

(1) Construct the averaged beat patterns using 5 beats for the respective atrial activation. Set $W=\mathcal{P}^2$ (W denotes a working space) and set $J_{\max}=0$.
(2) Choose $\boldsymbol{\vartheta}\in W$ and decompose the averaged activation patterns using $\boldsymbol{\vartheta}$ in the lattice implementation of the described wavelet-packet tree.
(3) Calculate the ℓ^1 norms of the output signals at the considered levels to obtain the feature vectors $\boldsymbol{\xi}^{\mathrm{ant}}(\boldsymbol{\vartheta})$ and $\boldsymbol{\xi}^{\mathrm{ret}}(\boldsymbol{\vartheta})$, respectively.

(4) Determine the *J divergence* of the feature vectors. If
$$J[\boldsymbol{\xi}^{\text{ant}}(\boldsymbol{\vartheta}),\boldsymbol{\xi}^{\text{ret}}(\boldsymbol{\vartheta})]>J_{\max}$$
set $J_{\max}=J[\boldsymbol{\xi}^{\text{ant}}(\boldsymbol{\vartheta}),\boldsymbol{\xi}^{\text{ret}}(\boldsymbol{\vartheta})]$ and $\hat{\boldsymbol{\vartheta}}=\boldsymbol{\vartheta}$.
(5) Remove $\boldsymbol{\vartheta}$ from W and repeat steps 2 to 4 until $W=\varnothing$.

AEE Classification Using Neural Networks

The feature vectors $\boldsymbol{\xi}^{\text{ant}}(\hat{\boldsymbol{\vartheta}})$ and $\boldsymbol{\xi}^{\text{ret}}(\hat{\boldsymbol{\vartheta}})$ are extracted in a manner, that they represent morphological dissimilarities of the distinct activation patterns. Now we need a classifier which indicates the underlying activation pattern of a given feature vector $\boldsymbol{\xi}(\hat{\boldsymbol{\vartheta}})$. Such a classifier c is a map

$$c:\mathcal{F}\rightarrow\mathcal{C},$$

where $\mathcal{C}=\{0,1\}$ represents the classification (or response) space of the two classes, i.e., the distinct atrial activations. Our classifier should be tolerant to slight changes of the features in $\mathcal{F}$ since we are dealing with signals of a biological origin where slight morphological changes are very likely to occur. In other words, we need the capability of a meaningful generalization. Further, the classification should be realized in a computationally efficient manner. A classifier c which match these conditions is a feed-forward neural network (FFNN) with one hidden layer. Such FFNNs have recently proven their capabilities for classifying bioelectric signals.[5,12,13,27]

FFNN Architecture. FFNN consists outward of $N^{(\mathrm{I})}=\dim\mathcal{F}=6$ formal input neurons and $N^{(\mathrm{O})}=1$ output neuron. The number of formal neurons in the hidden layer was determined empirically. Here the restriction to $N^{(\mathrm{H})}=4$ neurons has proven to be optimal in view of the network performance and, at the same time, its complexity. For an implementation in an implantable device a network of a low complexity is needed such that a small number of hidden neurons is desirable. With four neurons we achieved the best performance of the network with respect to the classification accuracy and in-class variability, respectively, when using a test set of data segments. We used the *Fermi* function, i.e., $T(\mu)=(1+e^{-\mu})^{-1}$ as sigmoidal transfer function of the neurons in the hidden layer.

An application of this network computes a value $\rho\in\mathbb{R}$ by

$$\rho=\sum_{p=1}^{N^{(\mathrm{H})}} w_p^{(\mathrm{O})}T\left[\sum_{i=1}^{N^{(\mathrm{I})}} w_{ip}^{(\mathrm{H})}\xi_i(\hat{\boldsymbol{\vartheta}})-\tau_p\right]. \tag{8}$$

Here $\boldsymbol{\tau}$ represents the threshold vector and $\mathbf{w}^{(\mathrm{O})}$ and $\mathbf{w}_p^{(\mathrm{H})}$ are the weights of the output and the hidden layer, respectively. To be more precise, $\mathbf{w}_p^{(\mathrm{H})}$ is the weight vector and τ_p is the threshold of the pth hidden formal neuron.

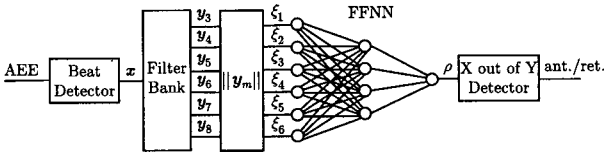

FIGURE 4. The complete AEE classification scheme.

Training of the FFNN. We applied the commonly used backpropagation method[15] for training the FFNN. For training, we used separately the preselected sets of the five antegrade and the five retrograde activations which make up the averaged atrial activation patterns. Let $\mathcal{A}^{\text{ant}}$ be the training set of feature vectors with respect to the five antegrade atrial activations. Analogously, $\mathcal{A}^{\text{ret}}$ denotes the training set of feature vectors of the five preselected retrograde atrial activations. Training means the determination of the weights and thresholds such that for all $\boldsymbol{\xi}(\hat{\boldsymbol{\vartheta}})\in\mathcal{A}^{\text{ant}}$ and $\boldsymbol{\xi}(\hat{\boldsymbol{\vartheta}})\in\mathcal{A}^{\text{ret}}$ with fixed outputs ρ^{ant} and ρ^{ret} the squared error

$$\sum_{\boldsymbol{\xi}^{\text{ant}}_{\text{ret}}(\hat{\boldsymbol{\vartheta}})\,\in\,\mathcal{A}^{\text{ant}}_{\text{ret}}}\left\{\rho^{\text{ant}}_{\text{ret}}-\sum_{p=1}^{N^{(\mathrm{H})}} w_p^{(\mathrm{O})}T\left[\sum_{i=1}^{N^{(\mathrm{I})}} w_{ip}^{(\mathrm{H})}\xi_i^{\text{ant}}_{\text{ret}}(\hat{\boldsymbol{\vartheta}})-\tau_p\right]\right\}^2$$

is minimal. Before training, the weights and thresholds of the FFNN were initialized with random numbers between -0.5 and 0.5. We had then trained the FFNN such that we have $\rho^{\text{ant}}=0$ for all $\boldsymbol{\xi}(\hat{\boldsymbol{\vartheta}})\in\mathcal{A}^{\text{ant}}$ and $\rho^{\text{ret}}=1$ for all $\boldsymbol{\xi}(\hat{\boldsymbol{\vartheta}})\in\mathcal{A}^{\text{ret}}$. The training was continued until the squared error converged to less than 1%.

As decision threshold $\kappa,\rho^{\text{ant}}<\kappa<\rho^{\text{ret}}$, which indicates whether physiological or pathological cardiac activities are present, we used $\kappa=0.5$ for all patients. Now we have an antegrade atrial activation if an application of the FFNN gives $\rho<\kappa$, i.e., class 0 and a retrograde activation if $\rho\geqslant\kappa$, i.e., class 1.

To improve the reliability of this decision, we applied a so-called *X out of Y* detector which was also used in Leong and Jabri.[12] Here a final decision is only made if X out of Y classifications of the FFNN are the same. In this way, incorrect classifications due to ectopic beats or artifacts, i.e., *outliers*, can be reduced. We used $X=6$ out of $Y=7$ beats. Our complete AEE classification scheme is shown schematically in Fig. 4.

RESULTS

Feature Extraction in AEEs

With the following examples we demonstrate the work of our feature extraction scheme.

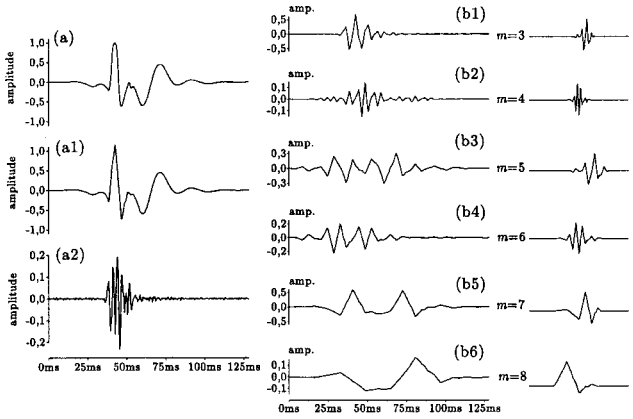

FIGURE 5. An exemplary decomposition: (a) the original signal; (a1) the reconstructed version of the signal without level $m=1$ and $m=2$; (a2) the reconstruction error; (b1)–(b2) the reconstructed subbands with the underlying basis function.

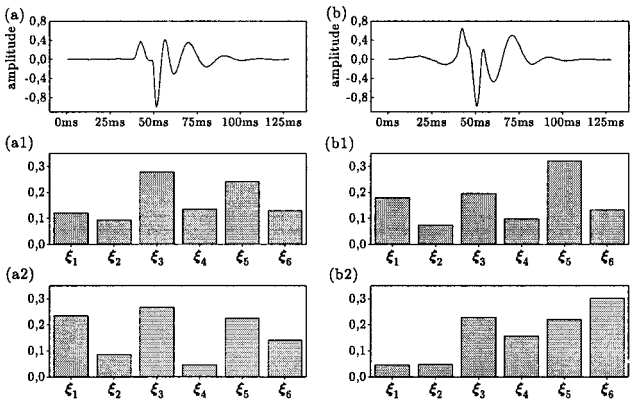

FIGURE 6. Extracted features in averaged activation patterns: (a) antegrade activation pattern; (b) retrograde activation pattern; (a1), (b1) the extracted features using a non-adapted decomposition; (a2), (b2) the extracted features using an adapted decomposition.

Decomposition Example. In Fig. 5(a) an exemplary decomposition of a selected beat is shown. Here we used the well known Daubechies filters[3] with six coefficients which correspond to $\boldsymbol{\vartheta}_{\mathrm{D6}}=(1.96185,0.49984)$ for the lattice implementation of the two-channel NP building blocks. In the middle column of Fig. 5 the expansions using $\mathbf{y}_3,\ldots,\mathbf{y}_8$ (thus, the reconstructed versions of the considered output signals of the filter bank) are shown in Figs. 5(b1)–Fig. 5(b6) in turn. On the right, the basis functions which span the corresponding subspaces of $\mathcal{S}$ and $\Omega_{0,0}$, respectively, with their appropriate shifts are illustrated. Please note that small levels m do not always correspond to high frequency atoms. The underlying wavelet packet tree $\Omega_{j,k}, j=1,\ldots,J, k=1,\ldots,2^{j-1}$, where the frequency does not monotonically increase with k, is called a *Paley ordered* tree.[29] Note further, that the sequences in Figs. 5(b5) and 5(b6) are the conventional wavelet representation of the signal on the decomposition levels $m=7$ and $m=8$, respectively. In Fig. 5(a1) the superposition of the signals Figs. 5(b1)–6(b6) is shown, hence, the reconstructed beat when the coefficients $\mathbf{y}_1,\mathbf{y}_2$ are discarded. In Fig. 5(a2) the resulting reconstruction error is illustrated. As noticeable, only finer details of the original signal are lost due to the reconstruction with a reduced number (only 1/4) of expansion coefficients.

Influence of the Adaptation. The given example can only provide a rough survey of the morphological features on our considered decomposition levels as the representation heavily depends on the underlying wavelet-packet basis. Therefore, the choice of a wavelet-packet basis which is properly adapted to the task at hand is crucial and can significantly improve the performance of the transform.

In the upper layer of Fig. 6 two averaged activation patterns are shown. The pattern in Fig. 6(a) represents an antegrade atrial activation, the pattern in Fig. 6(b) represents a retrograde one. In Fig. 6(a1) and Fig. 6(b1) the corresponding feature vectors $\boldsymbol{\xi}^{\mathrm{ant}}(\boldsymbol{\vartheta}_{\mathrm{D6}})$ and $\boldsymbol{\xi}^{\mathrm{ret}}(\boldsymbol{\vartheta}_{\mathrm{D6}})$, respectively, are shown as example for an arbitrary non-adapted initialization of the filter bank. The feature vectors $\boldsymbol{\xi}^{\mathrm{ant}}(\boldsymbol{\vartheta}_{\mathrm{D6}})$ and $\boldsymbol{\xi}^{\mathrm{ret}}(\boldsymbol{\vartheta}_{\mathrm{D6}})$ do not differ significantly. Indeed we have a small *J divergence*: $J[\boldsymbol{\xi}^{\mathrm{ant}}(\boldsymbol{\vartheta}_{\mathrm{D6}}),\boldsymbol{\xi}^{\mathrm{ret}}(\boldsymbol{\vartheta}_{\mathrm{D6}})]=0.09$ [we used the natural logarithm in Eq. (6) for the numerical experiments in this section]. In Figs. 6(a2) and 6(b2) we applied the angles $\hat{\boldsymbol{\vartheta}}$. Now the feature vectors $\boldsymbol{\xi}^{\mathrm{ant}}(\hat{\boldsymbol{\vartheta}})$ and $\boldsymbol{\xi}^{\mathrm{ret}}(\hat{\boldsymbol{\vartheta}})$ are highly dissimilar yielding a large *J divergence*: $J[\boldsymbol{\xi}^{\mathrm{ant}}(\hat{\boldsymbol{\vartheta}}),\boldsymbol{\xi}^{\mathrm{ret}}(\hat{\boldsymbol{\vartheta}})]=0.60$. In contrast to the time-domain representation only a few scale features represent clearly the discriminating information of the distinct activation patterns.

Performance of the AEE Classification Scheme

A total of 254 data segments (antegrade: 131, retrograde: 123) of 10 s were obtained from 30 patients (28 with AV nodal tachycardia, 2 with monomorphic VT with retrograde conduction). From the individual patient, the data segments were obtained with a time delay and five beats of the respective atrial activation were selected to provide the training sets $\mathcal{A}^{\mathrm{ant}}$ and $\mathcal{A}^{\mathrm{ret}}$ and the averaged antegrade and retrograde activation patterns, respectively. These beat patterns were visually controlled to avoid the inclusion of ectopic beats and artifacts in the training set. Using the averaged patterns, the angles $\hat{\boldsymbol{\vartheta}}$ were determined. The FFNN was then trained with feature vectors $\boldsymbol{\xi}(\hat{\boldsymbol{\vartheta}})\in\mathcal{A}^{\mathrm{ant}}$ and $\boldsymbol{\xi}(\hat{\boldsymbol{\vartheta}})\in\mathcal{A}^{\mathrm{ret}}$.

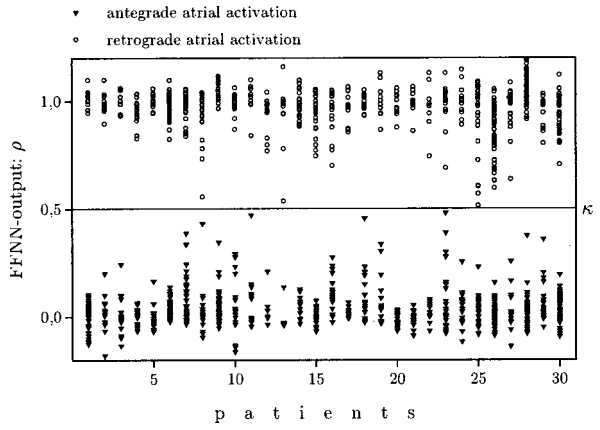

FIGURE 7. The results of the FFNN for all classified data segments.

Application Results. Our AEE classification scheme was applied to seven consecutive beats of each data segment which were not used for the adaptation and training of the FFNN, respectively, i.e., a test set of beats which is independent from the training set. 234 data segments were classified by the scheme and 20 data segments were discarded by the *X out of Y* detector. For the classified data segments, the outputs of the FFNN are shown in Fig. 7 for all sets of $X=6$ beats underlying the classification. A summary and statistical analysis of these results is given in Table 1 (SD: standard deviation). All individual atrial activations and data segments, respectively, were classified correctly with respect to our threshold $\kappa=0.5$. Thus, a classification accuracy of 100%, i.e., 100% sensitivity and 100% specificity, was achieved by our scheme in an automated analysis of the test set. In some patients a relatively large variance of the FFNN output can be observed. In patient No. 26 an unstable arrhythmia was recognized which caused the large variance. In some patients the endocardial recordings were of a bad quality since the AEEs were obtained from acute leads during an electrophysiological examination where respiration or movement of the electrode catheter can affect the AEE morphology. However, the overall variance seems to be small in view of the biological nature of the signals.

Rate Independence. In patient P1, P6, P9, and P30 the AEE was obtained during sinus rhythm and base line (BL) and after adrenergic stimulation (AS) with atropine and/or orciprenaline. After the stimulation, we had mean atrial cycle length reduction (CLR) of 40% compared to BL. Here no significant influence of the increasing heart rates on the FFNN output was observed. Details of this analysis are given in Table 2.

TABLE 1. FFN results for ll patients.

	ρ_{min}	ρ_{max}	ρ_{mean}	SD	Activations
Antegrade:	−0.45	0.48	0.03	0.09	726
Retrograde:	0.51	1.54	0.98	0.13	678

TABLE 2. $\rho_{mean}\pm$ SD for sinus rhythm at BL and after AS.

	P1	P6	P9	P30
CLR	40%	51%	31%	36%
BL	0.02±0.06	0.01±0.03	0.03±0.05	0.03±0.05
AS	−0.01±0.06	0.04±0.03	0.05±0.09	0.05±0.07

DISCUSSION

In the presented paper a new hybrid method for a classification of AEEs representing antegrade and retrograde atrial activation patterns is proposed. We used an adapted wavelet packet decomposition for feature extraction followed by a FFNN based classification. This method is new to the area of endocardial signal analysis.

The innovative approach of using an adapted decomposition technique, thus a tailor-made endocardial electrogram representation for individual patient, might contribute to overcome problems of known morphological endocardial electrogram analysis methods. For instance, in Leong and Jabri[12] a patient-dependent method is proposed which utilizes the time-domain representation of endocardial electrograms as neural network input to provide a classification of sinus rhythm and VT with 1:1 retrograde conduction. This method suffers from the fact that the morphological dissimilarities in endocardial electrograms representing distinct activation patterns are hardly to capture in the time domain, e.g., compare Figs. 6(a) and 6(b). For similar morphologies of the distinct atrial activation patterns this results in a false classification.[12]

In contrast to the Fourier transform based algorithm which is proposed in Minami *et al.*[13] for feature extraction in endocardial electrograms, the features which make up our feature space are extracted in a way, that they guarantee an illumination of the discriminating information in the distinct activation patterns. The use of an adapted basis is the major advantage of our feature extraction scheme in comparison to the Fourier transform which is restricted to fixed basis functions. Using the adapted basis, the discriminatory power is provided by the transform which individually maximizes the *J divergence* of the multilevel concentration of distinct activation patterns. Therefore, the whole classification scheme takes into account the particular AEE morphology of the individual patient. The resulting feature vectors are of a low dimension such that an FFNN of a low complexity can be applied.

A problem that often occurs when using time-domain template matching methods is a false classification if the selected activation is not centered in the same fashion as the template. Here computationally demanding selection enhancement methods like the *best fit alignment*[22] for the correlation waveform analysis are necessary. To handle the alignment problem in our scheme, we preferred the concentration on a decomposition level, i.e., on a specific frequency band, rather than the transient information directly. But of course, due to the use of the multirate operations the scheme is still shift variant. A shift invariance can be achieved by undecimted filter banks which are related to wavelet frames.[2] However, these decompositions are very computationally demanding. The construction of more efficient approximated shift-invariant decompositions[11] seems to be a branch of interesting further research in the area of shift-invariant endocardial signal analysis. Please also note, that the ability for an adjustment of the atoms to discriminating features being compact in time is involved during adaptation. Here local features are involved to spread the multilevel concentration of the distinct activation patterns. The concentration in specific frequency bands of a multirate filter bank decomposition for feature extraction followed by a FFNN has also recently proven to be powerful for a classification of electrogastrograms.[27]

We applied a wavelet-packet decomposition which can be seen as a generalized version of wavelet expansion where the filter bank tree is restricted to have an octave-band structure. In contrast to wavelet expansions, wavelet-packet decompositions offer more flexibility and an enhancement in the frequency resolution at the price of a poorer time resolution due to a larger support of the basis functions on detailed (or high frequency) decomposition levels. However, the use of atoms which allow for an accurate transient localization of features it is not necessary—and in fact not desirable—for our task since the transient information suffers from the alignment problem which is discussed earlier. Therefore, we preferred the flexible wavelet-packet decomposition scheme over the conventional wavelet expansion.

We also like to emphasize that we stuck to the very same decomposition tree for all patients and used the lattice parameterization which provides a very large set adaptable wavelet-packet bases of this tree. In known wavelet-packet schemes only a small number of smooth filters is used and often the tree is adapted.[16,29] However, a smoothness constraint is not necessary for our task and the complete architecture of the classification scheme must be individually adjusted if the decomposition tree varies from patient to patient. A fact which is not desirable when considering implementation strategies. Therefore, we used a large set of arbitrary bases of a fixed tree rather than a tree adaptation. In our scheme only an adjustment of the lattice angles provides the adaptation of the decomposition such that we can use a fixed architecture for all patients.

Please note that the tree structure utilized for realizing a wavelet-packet decomposition depends on the preprocessing of the endocardial signals, i.e., filtering and sampling. Therefore, the decomposition tree suggested in this paper is only appropriate when the same preprocessing of the data was applied. However, due to the flexibility of wavelet-packet decompositions such a tree can easily be modified and adapted to another preprocessing. If necessary, the FFNN architecture must then be adjusted to the modified decomposition tree.

We applied orthonormal expansions which involve the use of perfect reconstruction filter banks. At first sight the perfect reconstruction condition seems not necessary for our task. However, orthonormal decompositions provide the whole information of a given signal in a nonredundant manner. Therefore, they guarantee that the subbands on each decomposition level carry different information, a desirable property for the extraction of signal features. Furthermore, in view of the current interest in endocardial electrogram compression algorithms[1] for ICDs, coding conditions can be added to our scheme without difficulty.

Enhanced detection criteria utilizing the endocardial electrogram morphology additional to the rate information require a supplementary computational load. In view of the limited energy resources of implantable devices, efficient implementation strategies of such methods are needed. Therefore, we preferred the adapted orthonormal decomposition which can be implemented using paraunitary filter banks over the computationally demanding integral wavelet transform. The latter one is also used successfully in hybrid wavelet-neural network systems—the so-called *wavelet networks*—for classifying biosignals.[5] The efficiency of filter banks based on lattice structure is well known[24,25] and has recently proven to be suitable for very large scale integrated implementations.[10] FFNNs allow for an efficient implementation due to their inherit parallelism and simplicity of the processing elements making them suitable for our purpose. The computationally demanding adaptation of the decomposition and the training of the FFNN are realized off-line. The classification algorithm itself is of low complexity. For the individual patient, only the lattice angles and FFNN parameters must be changed to implement a sophisticated, patient adjusted algorithm.

Limitations. We aimed at the classification of antegrade and retrograde atrial activation which can be used to differentiate VT with 1:1 retrograde conduction from sinus tachycardia. This method is not suitable for a discrimination of VT from supraventricular reentrant tachycardia with retrograde activation such as AV nodal reentrant tachycardia or AV junctional tachycardia. How-

ever, both arrhythmias are very rare in the typical ICD populations and can be cured by radiofrequency ablation. We like to emphasize that all patients entered our study were in a resting state and supine position. The influence of different lead positions, the presence of antiarrhythmic drugs, and changing electrophysiological properties of the cardiac tissue to our classification scheme is not known. Further, the AEEs were obtained from acute leads during an electrophysiological examination. Possible effects of lead maturation were not studied. As for all morphology based classification techniques, the choice of the training patterns of the individual patient is crucial and affects the performance of our scheme. With the given data it cannot be said whether the scheme performs even better if another filtering is applied such that more low frequency information of the raw signals is included in the analysis.

CONCLUSION

We have developed a new hybrid method for classifying antegrade and retrograde atrial activation patterns in AEEs based on adapted wavelet-packet decompositions and FFNNs. This method can be used to distinguish sinus tachycardia from VT with 1:1 retrograde conduction, an unsolved problem for rate based algorithms currently used in dual-chamber ICDs. In an automated analysis, no false classification was made by our classification scheme such that a high accuracy was concluded. The application of the proposed method seems also to be promising for other morphological classification tasks in electrocardiology. However, with the given limitations, further investigations are needed to evaluate whether our method will offer the same performance in every day clinical use.

NOMENCLATURE

$\mathbb{R}$	the set of real numbers
$\mathbb{N}$	the set of natural numbers
dim	the dimension of a space
ℓ^p	the space of pth power summable sequences
$\|\cdot\|_{\ell^p}$	the norm on ℓ^p
I	the identity operator on $\mathbb{R}^K$
$\oplus$	direct sum
$\mathbf{H}_{\text{pol}}(z)$	polyphase matrix of a two channel analysis bank, that is, $\mathbf{H}_{\text{pol}}(z)=\begin{pmatrix} H_{00}^{\text{p1}}(z) & H_{01}^{\text{p1}}(z) \\ H_{10}^{\text{p1}}(z) & H_{11}^{\text{p1}}(z) \end{pmatrix}$, where $H_{\mu\nu}^{\text{p1}}(z), \mu, \nu \in \{0,1\}$ are the polyphase components of the analysis filters
$\mathbf{R}$	orthogonal rotation matrix
diag$[a,b]$	2×2 diagonal matrix with elements a, b
$\mathbf{I}$	2×2 identity matrix
$\tilde{\mathbf{Q}}(z)$	paraconjugation of $\mathbf{Q}(z)$, that is $\mathbf{Q}_*^T(z^{-1})$
argmax	the argument of the maximum, i.e., $\hat{x} = \text{argmax}\{f(x) \mid x \in X\}$, $f(\hat{x}) \geqslant f(x) \forall x \in X$

The multirate basic building blocks:

M-fold decimator	$y[\cdot] = \Sigma_{k\in\mathbb{Z}} x[k] h[M\cdot - k]$
L-fold interpolator	$y[\cdot] = \Sigma_{k\in\mathbb{Z}} x[k] g[\cdot - kL]$

REFERENCES

[1] Coggins, R. J., and M. A. Jabri. A low-complexity intracardiac electrogram compression algorithm. *IEEE Trans. Biomed. Eng.* 46:83–91, 1999.

[2] Cvetkovic, Z., and M. Vetterli. Oversampled filter banks. *IEEE Trans. Signal Process.* 46:1245–1255, 1998.

[3] Daubechies, I. Orthonormal bases of compactly supported wavelets. *Commun. Pure Appl. Math.* 41:906–966, 1988.

[4] Delsarte, P. H., B. Macq, and D. T. M. Slock. Signal adapted multiresolution transforms for image coding. *IEEE Trans. Inf. Theory* 38:897–903, 1992.

[5] Dickhaus, H., and H. Heinrich. Classifying biosignals with wavelet networks. *IEEE Eng. Med. Biol. Mag.* 15:105–111, 1996.

[6] Intraton, N., Q. Huynh, Y. Wong, and B. H. K. Lee. Wavelet feature extraction for discrimination tasks. Proceedings of the Canadian Workshop on Information Theory, Toronto, 1997, pp. 83–86.

[7] Jung, J., D. Strauss, T. Sinnwell, H. Hohenberg, R. Fries, H. Wern, H. Schieffer, and A. Heisel. Assessment of intersignal variability for discrimination of atrial fibrillation from atrial flutter. *PACE* 21:2426–2430, 1998.

[8] Jung, J., D. Strauss, T. Sinnwell, H. Hohenberg, R. Fries, H. Wern, H. Schieffer, and A. Heisel. Identification of Ventricular Tachycardias by Means of Fast Wavelet Analysis. In: IEEE Computers in Cardiology (25), edited by A. Murray and S. Swiryn, New Jersey: 1998, pp. 21–24.

[9] Khadra, L., A. S. Al-Fahoum, and H. AL-Nashash. Detection of life-threatening cardiac arrhythmias using the wavelet transformation. *Med. Biol. Eng. Comput.* 35:626–632, 1997.

[10] Kim, J. T., Y. H. Lee, T. Isshiki, and H. Kunieda. Scalable VLSI architectures for lattice-structure-based discrete wavelet transform. *IEEE Trans. Circuits Syst., II: Analog Digital Signal Process.* 45:1031–1043, 1998.

[11] Kingsbury, N. G. Shift invariant properties of the dual-tree complex wavelet transform. Proc. IEEE Conf. on Acoustics, Speech and Signal Processing, paper SPTM 3.6, 16–19 March 1999.

[12] Leong, P. H. W., and M. A. Jabri. Matic—An intracardiac tachycardia classification system. *PACE* 15:1317–1331, 1992.

[13] Minami, K., H. Nakajima, and T. Toyoshima. Real-time discrimination of ventricular tachyarrhythmias with Fourier transform neural networks. *IEEE Trans. Biomed. Eng.* 46:179–185, 1999.

[14] Nain, M., N. Saoudi, D. Kroiss, and B. Letac. Automatic arrhythmia identification using analysis of the atrioventricular association. Application to a new generation of implantable defibrillators. Participating centers of the Automatic Recognition of Arrhythmia Study Group. *Circulation* 95:967–973, 1997.

[15] Ripley B. D. Pattern Recognition and Neural Networks. New York: Cambridge University Press, 1996.

[16] Saito, N., and R. R. Coifman. Local Discriminat Bases. In:

Mathematical Imaging: Wavelet Applications in Signal and Image Processing, edited by A. F. Laine and M. A. Unser, 1994.
[17] Schaumann, A., F. von zur Mühlen, B. D. Gonska, and H. Kreuzer. Enhanced detection criteria in implantable cardioverter-defibrillators to avoid inappropriate therapy. *Am. J. Cardiol.* 78:42–50, 1996.
[18] Strang G., and T. Nguyen. Wavelets and Filter Banks. Wellesley, MA: Wellesley, Cambridge, 1996.
[19] The Antiarrhythmics Versus Implantable Defibrillators (AVID) Investigators. A comparison of antiarrhythmic drug therapy with implantable defibrillators in patients resuscitated from near fatal ventricular arrhythmias. *N. Engl. J. Med.* 337:1576–1583, 1997.
[20] Throne, R. D., J. M. Jenkins, and L. A. DiCarlo. The bin area method: A computationally efficient technique for analysis of ventricular and atrial intracardiac electrograms. *PACE* 13:1286–1297, 1990.
[21] Throne, R. D., J. M. Jenkins, and L. A. DiCarlo. Evaluation of area of difference algorithms for detecting ventricular tachycardia using electrogram morphology. *Proc. Annu. Conf. IEEE Eng. Med. Biol. Soc.* 12-2:584–585, 1990.
[22] Throne, R. D., J. M. Jenkins, S. A. Winston, C. J. Finelli, and L. A. Di-Carlo. Discrimination of retrograde from antegrade atrial activation using intracardiac electrogram waveform analysis. *PACE* 12:1622–1630, 1989.
[23] Timmis, G. C., D. C. Westveer, D. M. Bakalyar, T. J. Pugsly, J. R. Steward, and S. Gordon. Discrimination of antegrade from retrograde atrial electrograms for physiologic pacing. *PACE* 11:130–140, 1988.
[24] Vaidyanathan, P. P. Multirate Systems and Filter Banks. Englewood Cliffs, NJ: Prentice-Hall, 1993.
[25] Vaidyanathan, P. P., and P. Q. Hoang. Lattice structures for optimal design and robust implementation of two-channel perfect reconstruction qmf filter banks. *IEEE Trans. Acoust., Speech, Signal Process.* 36:81–94, 1988.
[26] Vetterli, M., and J. Kovačević. Wavelets and Subband Coding. Englewood Cliffs, NJ: Prentice-Hall, 1995.
[27] Wang, Z., Z. He, and J. D. Z. Chen. Filter banks and neural networks-based feature extraction and automatic classification of electrogastrogam. *Ann. Biomed. Eng.* 27:88–95, 1999.
[28] Weber, M., D. Böcker, D. Bansch, J. Brunn, M. Castrucci, R. Gradaus, G. Breithardt, and M. Block. Enhanced detection criteria in implantable cardioverter-defibrillators to avoid inappropriate therapy. *J. Cardiovasc. Electrophysiol*. 10:145–153, 1999.
[29] Wickerhauser, M. V. Adapted Wavelet Analysis Form Theory to Software. Wellesley, MA: A. K. Peters, Ltd., 1994.